



HAL
open science

Volcanic terrain and the possible periglacial formation of “excess ice” at the mid-latitudes of Utopia Planitia, Mars

R.J. Soare, B. Horgan, Susan J. Conway, C. Souness, M.R. El-Maarry

► To cite this version:

R.J. Soare, B. Horgan, Susan J. Conway, C. Souness, M.R. El-Maarry. Volcanic terrain and the possible periglacial formation of “excess ice” at the mid-latitudes of Utopia Planitia, Mars. *Earth and Planetary Science Letters*, 2015, 423, pp.182-192. 10.1016/j.epsl.2015.04.033 . insu-02274301

HAL Id: insu-02274301

<https://insu.hal.science/insu-02274301>

Submitted on 8 Jan 2021

HAL is a multi-disciplinary open access archive for the deposit and dissemination of scientific research documents, whether they are published or not. The documents may come from teaching and research institutions in France or abroad, or from public or private research centers.

L'archive ouverte pluridisciplinaire **HAL**, est destinée au dépôt et à la diffusion de documents scientifiques de niveau recherche, publiés ou non, émanant des établissements d'enseignement et de recherche français ou étrangers, des laboratoires publics ou privés.

Volcanic terrain and the possible periglacial formation of “excess ice” at the mid-latitudes of Utopia Planitia, Mars

R.J. Soare,¹ B. Horgan,² S.J. Conway,³ C. Souness,⁴ and M.R. El-Maarry⁵

¹Department of Geography, Dawson College, Montreal, Canada, H3Z 1A4
(rsoare@dawsoncollege.qc.ca)

²Earth, Atmospheric & Planetary Sciences, Purdue University,
West Lafayette, Indiana, USA 47907-2051

³Department of Physical Sciences, Open University,
Milton Keynes, UK, MK7 6AA

⁴Centre for Glaciology, Department of Geosciences, Aberystwyth University,
Aberystwyth, UK, SY23 3DB

⁵Physikalisches Institut, Bern Universität, Berne, Switzerland, 3012

1

2

3

4

5

6 **Pages-34**

7 **Figures-7**

8 **Tables-0**

9 **Key Words-Mars: climate, atmosphere, surface**

10

11

12 **Abstract**

13 At the mid-latitudes of Utopia Planitia (*UP*), Mars, a suite of spatially-associated
14 landforms exhibit geomorphological traits that, on Earth, would be consistent with periglacial
15 processes and the possible freeze-thaw cycling of water. The suite comprises small-sized
16 polygonally-patterned ground, polygon-junction and -margin pits, and scalloped, rimless
17 depressions. Typically, the landforms incise a dark-toned terrain that is thought to be ice-rich.
18 Here, we investigate the dark-toned terrain by using high resolution images from the *HiRISE*
19 as well as near-infrared spectral-data from the *OMEGA* and *CRISM*. The terrain displays
20 erosional characteristics consistent with a sedimentary nature and a unique spectral-shape that
21 could be indicative of weathered basaltic-tephra. We also describe volcanic terrain that is
22 dark-toned and periglacially-modified in the Kamchatka mountain-range of eastern Russia.
23 The terrain is characterised by weathered tephra inter-bedded with snow, ice-wedge polygons
24 and near-surface excess ice. The excess ice forms in the pore space of the tephra as the result
25 of snow-melt infiltration and, subsequently, *in-situ* freezing. Based on this possible analogue,
26 we construct a three-stage mechanism that explains the possible ice-enrichment of a broad
27 expanse of dark-toned terrain at the mid-latitudes of *UP*: (1) the dark-toned terrain
28 accumulates and forms via the regional deposition of sediments sourced from explosive
29 volcanism; (2) the volcanic sediments are blanketed by atmospherically-precipitated (H_2O)
30 snow, ice or an admixture of the two, either concurrent with the volcanic-events or between
31 discrete events; and, (3) under the influence of high obliquity or explosive volcanism,
32 boundary conditions tolerant of thaw evolve and this, in turn, permits the migration, cycling
33 and eventual formation of excess ice in the volcanic sediments. Over time, and through
34 episodic iterations of this scenario, excess ice forms to decametres of depth.

35 **1. Introduction**

36 At the mid-latitudes (38-45° N; 85-93° E) of Utopia Planitia (*UP*), Mars, an expansive

37 reach of dark-toned terrain (**Fig. 1a**) is incised by three spatially-associated landforms (**Fig.**
38 **2a-c**) whose geomorphological traits, were they observed on Earth, would be consistent with
39 periglacial processes, the possible freeze-thaw cycling of water and, most importantly, the
40 presence of excess ice (**Fig. 2d**). Excess ice occurs where “the volume of ice in the ground
41 *exceeds* the total pore-volume that the ground would have under unfrozen-conditions” (Harris
42 et al., 1988).

43 The suite of putative periglacial-landforms (*PPLs*) comprises: (a) small-sized ($\leq 50\text{m}$)
44 and non-sorted polygonally-patterned ground (Mellon, 1997; Seibert and Kargel, 2001;
45 Morgenstern et al., 2007; Soare et al., 2008, 2009, 2012b; Lefort et al., 2009; Levy et al.,
46 2009a,b; Hauber et al., 2011; Ulrich et al., 2011); (b) multi-metre scale polygon-junction and
47 margin pits (Wan Bun Tseung and Soare, 2006; Morgenstern et al., 2007; Séjourné et al.,
48 2010); and, (c) scalloped depressions that are rimless, flat-floored, metres to tens of
49 decametres deep and metres to kilometres in their long axes (Costard and Kargel;
50 Morgenstern et al., 2007; Soare et al., 2007, 2008, 2011; Lefort et al., 2009; Ulrich et al.,
51 2010; Séjourné et al., 2011, 2012).

52 There is widespread agreement amongst Mars researchers that the scalloped
53 depressions are thermokarst-like basins (*alases*) that formed, along with the other two *PPLs*,
54 in response to the thermal destabilization of ice-rich terrain (e.g. Morgenstern et al., 2007;
55 Soare et al., 2007, 2008; Lefort et al., 2009; Séjourné et al., 2011, 2012). Opinions diverge,
56 however, in response to two questions:

57 (1) Do the thermokarst-like basins form by means of (a) melting and evaporation or
58 (b) sublimation?

59 (2) By which means did the dark-toned terrain cross-cut by the *PPLs* become ice-
60 rich?

61 Although the answer to the first question remains open-ended, we believe that the data and

62 observations presented in this study can begin to address and, perhaps answer, the second
63 question.

64 Numerous researchers propose that the *PPLs* in mid-*UP* originate and evolve in an
65 extremely young and ubiquitous light-toned mantle comprised of ice-dust (e.g. Morgenstern
66 et al., 2007; Lefort et al., 2009; also, Levy et al., 2009a-b, 2010). By contrast, our previous
67 observations show that the *PPLs* generally incise terrain that is dark, not light, in tone (Soare
68 et al., 2012a-b); moreover, where the two differently-toned terrains are proximal, we find that
69 the dark-toned terrain is at a lower relative-elevation than the light-toned terrain, suggesting
70 that the *PPLs* pre-date rather than post-date the mantle (Soare et al., 2012a-b). Thus, the dark-
71 toned terrain is not derived from the (possibly) ice-rich light-toned mantle, but is a separate
72 and older ice-rich unit.

73 Here, we use an assemblage of high-resolution images and spectral data to investigate
74 the dark and light-toned terrains. We show that the dark-toned and possibly “ice-rich” terrain
75 in mid-*UP* has a unique spectral-shape that is consistent with weathered basaltic-tephra. Next,
76 we present and describe a possible terrestrial-analogue comprised of a dark toned and
77 periglacially-modified volcanic terrain in the Kamchatka mountain-range of eastern Russia.
78 The terrain is typified by ice-wedge polygons, weathered volcanic tephra inter-bedded with
79 snow, and near-surface excess ice; it forms in the pore space of the tephra as the result of
80 snow-melt infiltration and, subsequently, *in-situ* freezing. We suggest that the Kamchatkan
81 terrain is a useful geological/geomorphological analogue of mid-*UP*. Consequently, we
82 construct a three-stage hypothesis modelled after the former that explains the volcanic origin
83 of the dark-toned terrain on Mars and its ice enrichment by the freeze-thaw cycling of surface
84 and near-surface melt-water.

85 **2. Methods**

86 In order to constrain the possible origin of excess ice in the dark-toned terrain of mid
87 *UP* we have used four datasets: (1) visible imagery from the High Resolution Imaging
88 Science Experiment (*HiRISE*, Mars Reconnaissance Orbiter; McEwen et al, 2007) and (2) the
89 Context Camera (*CTX*, Mars Reconnaissance Orbiter; Malin et al., 2007); (3) km-scale
90 visible to near-infrared spectral context from the Observatoire pour la Mineralogie, l'Eau, les
91 Glaces, et l'Activité (*OMEGA*, Mars Express; Bibring et al., 2005); and, (4) decameter-scale
92 visible to near-infrared spectra from the Compact Reconnaissance Imaging Spectrometer for
93 Mars (*CRISM*, Mars Reconnaissance Orbiter; Murchie et al., 2007).

94 Morphology and (visible) surface-properties were evaluated on a regional scale using
95 a mosaic of *CTX* images (6m/pixel, adapted from Soare et al., 2012b) (**Fig. 1c**). *HiRISE*
96 images (25-50cm/pixel) were used as required to investigate and highlight morphologies and
97 surface textures at higher resolutions (**Figs. 2, 5**).

98 For context, visible to near-infrared (0.35-2.5 μ m) spectral properties of the regional
99 surface were identified by means of a (1km/pixel) *OMEGA* mosaic covering 60-120°E and
100 30-65°N. The mosaic was constructed from all publicly available *OMEGA* observations,
101 calibrated using the SOFT04 software package, converted to an estimated Lambert albedo,
102 then filtered and ordered using the methods described by Ody et al. (2012). The visible
103 portion of each spectrum was adjusted for best spectral alignment with the near-infrared
104 portion of the spectrum, as described in detail in Horgan et al. (2014). This step is necessary
105 because the visible and near-infrared portions of the spectra are collected by two different
106 CCD's with slightly different viewing geometries and calibrations, thus leading to small
107 (typically 0-3%) offsets between their spectra. **Figures 1b and 1d** shows the magnitude of
108 the spectral slope of the *OMEGA* spectra in this mosaic between 0.77 and 1.30 μ m, calculated
109 as the ratio of the three closest channels to each of these wavelengths. This slope parameter
110 spans both the visible and near-infrared portions of the *OMEGA* spectra, and thus would be

111 affected by poor spectral alignment at the visible/near-IR join. However, the alignment step
112 above accounts for most alignment issues, as demonstrated by the fact that the parameter
113 does not vary significantly across image boundaries in the map.

114 Local spectral variations were investigated using *CRISM* observations (18m/pixel), as
115 shown in **Figure 3**, which were downloaded from the Planetary Data System at the TRR3
116 calibration level. Further processing to estimated Lambertian-albedo utilized the *CRISM*
117 Analysis Toolkit for *ENVI* (Seelos et al., 2011), including photometric and scaled volcano
118 scan atmospheric corrections. No additional spectral processing was applied to these images
119 (e.g., ratios, continuum removal, etc.), so all spectra shown in **Figure 3** are unmodified
120 albedo spectra. Two continuous groups of channels near 1 and 2 μm were removed due to
121 noise near the visible/near-IR join and residual features from the atmospheric correction (e.g.,
122 Seelos et al., 2014). All spectra are averages of at least 3x3 up to 10x10 pixel areas.

123 **3. Spectral properties of the dark-toned terrain in UP**

124 Previous studies have shown that the low-albedo regions of the northern plains,
125 principally in Acidalia and Utopia Planitiae, show spectra that are highly homogeneous: in
126 the near-infrared, the spectra slope linearly downward to longer wavelengths (a “blue” slope;
127 e.g., Mustard et al., 2005). In some locations, the spectra are more sloped at the shorter
128 wavelengths than at the longer ones, creating a nonlinear “concave up” shape (Horgan and
129 Bell, 2012; Horgan et al., 2013). A simple method for identifying these concave up spectra is
130 to map the spectral slope between 0.77 and 1.3 μm , as shown in **Figures 1b and 1d**.

131 Unlike other dark regions of Mars, the northern plains do not exhibit strong
132 absorption bands resulting from the iron in mafic minerals (Mustard et al., 2005; Poulet et al.,
133 2008); typically, these occur near 1 and sometimes also 2 μm (e.g., Adams, 1968). Our study
134 region is dominated by dark surface sediments that exhibit similar spectral characteristics to
135 other locations in the northern plains, including low albedo, blue and often concave up

136 spectral slopes, and no or very shallow iron absorption-bands, as demonstrated by spectra 1-
137 3, 6, and 8 in **Figure 3**. As discussed in greater detail below, these characteristics are
138 consistent with weathered glass-rich deposits.

139 Linear blue spectral-slopes can be indicative of coatings deposited during aqueous
140 alteration (silica or oxide coatings) or dry oxidative weathering (oxide rinds) (Kraft et al.,
141 2007; Milliken et al., 2008; Minitti et al., 2007; Salvatore et al., 2013). They also could be
142 due to optically-thin layers of bright dust on a dark substrate (Fischer and Pieters, 1993).
143 Based on these spectral analogues, the linear blue spectral-slopes found throughout much of
144 the northern plains have been interpreted as either oxide coatings or rinds (Mustard et al.,
145 2005; Poulet et al., 2008; Salvatore et al., 2013).

146 On the other hand, nonlinear concave up slopes at wavelengths below $1.3\mu\text{m}$ are not
147 caused by these effects, but instead are often associated with leached rinds on glass, usually
148 due to acidic aqueous alteration (Minitti et al., 2007; Seelos et al., 2010; Horgan and Bell,
149 2012; Horgan et al., 2013). For example, **Figure 4** shows spectra of basaltic glasses at Mauna
150 Kea, Hawaii, including cooling rinds on lavas, glassy lavas, and tephra. Unaltered ash
151 exhibits broad absorption bands and often a red spectral slope; by contrast, ash and glass
152 exposed to acidic weathering conditions (on Mauna Kea, due to volcanic sulfur emissions)
153 exhibit no or very weak bands and a concave-up spectral slope that, sometimes, also is blue.
154 Although this spectral signature usually is associated with sands or larger sedimentary-grains,
155 it dominates the bulk spectrum of ash even when the ash is poorly sorted (**Fig. 4c**).

156 In the northern plains, concave-up slopes have been shown to be primarily associated
157 with dune fields and other dark surface sediments (Horgan and Bell, 2012). One key line of
158 evidence for the leached-glass interpretation of the concave-up spectral slopes is their
159 common association with weak iron-absorption bands centered near $1.15\ \mu\text{m}$ (Horgan and
160 Bell, 2012); these are uniquely consistent with iron-bearing glass (*e.g.*, Adams et al., 1974).

161 These 1.15 μm bands are the only mafic absorption bands observed in the dark surface
162 sediments of the northern plains, and are observed in about 5% of OMEGA spectra in
163 Acidalia and Utopia, in nearly 30% of the north-polar sand sea, and are highly correlated with
164 concave-up slopes (Horgan and Bell, 2012; Horgan et al., 2014). Furthermore, areas that
165 exhibit the strongest concave-up slopes do not exhibit iron absorption bands, consistent with
166 obscuration of the glass substrate by a leaching rind (Minitti et al., 2007; Horgan and Bell,
167 2012; Horgan et al., 2013). Although the dark-toned surface sediments in our study region
168 typically do not exhibit clear and diagnostic iron absorption bands due to glass or other
169 minerals, they are otherwise spectrally very similar to other widespread areas in the northern
170 lowlands previously interpreted as weathered glass. Thus, we hypothesize that the dark
171 surface sediments in our study region are also weathered glass.

172 In our study region, there are indications of spectral diversity at depths below the
173 dark-toned terrain, suggesting that the dark sediments that the PPL's incise are limited in
174 their thickness, on the order of decameters. Some still dark but slightly lighter-toned sub-
175 surface units exposed in the walls of craters exhibit a different spectral shape than the dark
176 surface sediments, with a broad absorption between 0.8 and 1.8 μm , such as spectra 4 and 5 in
177 **Figure 3**. These spectra are similar to spectra from crater walls in central and southern
178 Acidalia Planitia; these are interpreted to be olivine-bearing (Salvatore et al., 2010). The \sim 1
179 μm absorptions of the buried units in *UP* are somewhat broader than in Acidalia, but could be
180 consistent with an olivine and/or glass-rich basalt, or some other mafic phase. These spectra
181 are observed in association with moderate-toned cliff-forming units and sediments that
182 appear to be derived from these units, including transverse aeolian-ridges and wind-streaks.
183 This suggests a sedimentary nature for this material as well as the dark terrain above, but the
184 origin and emplacement history is less well-constrained in these lower units.

185 By contrast, the light-toned "mantle" that resides to the south and on the margins of

186 the dark-toned terrain displays a signature that is not consistent with a ferrous composition
187 but rather a more typically ferric and “dusty” composition (spectrum 7 in **Figure 3**).
188 Additionally, we do not observe any spectral indications of ice in this mantle. Spectrally, this
189 is distinct from the dark-toned terrain incised by the *PPLs* and identifies the light-toned
190 terrain as being geologically distinct from the latter. This result is in line with our previous
191 stratigraphical observations suggesting that the light-toned mantle postdates the dark terrain,
192 and is therefore not the cause of the ice enrichment in this region (Soare et al., 2012a-b).

193 **4. Interpretation of sediment origin**

194 The dark-toned terrain exhibits characteristics that are consistent with erosion and
195 aeolian transport of a sedimentary unit, including wind streaks, accumulation of dark
196 sediments (**Fig. 5**), and one dune field located just north of our study region (Horgan and
197 Bell, 2012). The dark toned terrain also exhibits possible layers in the walls of some
198 scalloped depressions (**Fig. 5**). If these dark-toned sediments in *UP* are indeed glass-rich, we
199 hypothesize that they may have originally formed either as impact-associated ejecta or
200 volcanoclastic sediments. In either scenario, the sediments may have been laid down directly
201 due to distal ballistic or atmospheric fallout, or may have been deposited elsewhere and then
202 transported to their current location via other sedimentary processes (fluvial/outflow, aeolian,
203 etc.). However, crater walls in this region do not exhibit the clear layers and flow-related
204 stratigraphic landforms that are observed in Acidalia Planitia and interpreted as evidence for
205 flood/fluvial deposits (Salvatore et al., 2014). Instead, crater walls in our study area exhibit
206 massive morphologies without clear layering. While this may be in part due to modification
207 and obscuration by the pervasive periglacial processes that have operated in our study area,
208 this observation leads us to favour an air fall-deposition model for the sediments in *UP*. This
209 hypothesis is also more consistent with the very Late Amazonian Epoch age for these

210 deposits than flood/fluvial deposition, as this time period post-dates outflow channel activity
211 (Tanaka *et al.*, 2003).

212 Several authors propose that there should be globally-distributed impact melt-droplets
213 (sub-mm size) on Mars even from relatively small craters (Lorenz 2000; Schultz and Mustard
214 2004). Given estimates of current cratering-rates, these same authors suggest that ejecta
215 layers on the order of tens of μm to mm thick could accumulate every $\sim 10^4$ - 10^5 years.
216 Derivatively, ejecta layers thick enough to be incised to tens or hundreds of metres of depth
217 by the scalloped depressions would require on the order of $\sim 10^8$ - 10^9 years to accumulate,
218 effectively approaching the full Amazonian Epoch time-period. This is inconsistent with the
219 most recent age-estimates of the surface in and around the mid-latitudes of *UP*, all of which
220 point to the terrain having been formed very recently, in the very Late Amazonian Epoch
221 (e.g. Mustard *et al.*, 2001; Head *et al.*, 2003; Milliken *et al.*, 2003; Tanaka *et al.*, 2005; Levy
222 *et al.*, 2009a-c; Madeleine *et al.*, 2009, 2014). Although an impact origin for the dark-toned
223 sediments cannot be ruled out, from a geochronological point of view, other sources may be
224 more plausible.

225 The glass-rich composition of the sediments is also consistent with tephra, more
226 particularly, ash, produced by explosive volcanism. The low albedo is also consistent with
227 many varieties of iron-bearing glass, and is reminiscent of dark and glass-rich volcanic plains
228 in Iceland (Arnalds, 2001; Horgan and Bell, 2012). Modeling of explosive volcanism on
229 Mars points to three key inferences: 1. massive eruptions have been commonplace through
230 the geological history of the planet; 2. eruptions on Mars probably were much more explosive
231 than on Earth due to lower atmospheric-pressure; and 3. dispersion of silt to sand-sized grains
232 of ash (by air fall) can be widespread, thick and layered (Wilson and Head, 2007; Kerber *et al.*
233 *et al.*, 2012). In particular, Kerber *et al.* (2012) demonstrate that the airfall deposition of ash
234 from an explosive event centred at Syrtis Major could reach the mid-latitudes of *UP* where

235 the dark-toned terrain is observed when Mars' obliquity is extreme. Other source regions
236 such as Arabia Terra are possible (Kerber et al., 2012) and further investigation is warranted.

237 Compared to an impact-melt origin, an explosive volcanic origin for these deposits
238 would imply a relatively short deposition-timescale. Moreover, if a major volcanic-event
239 coincided with (or perhaps motivated) a period of enhanced precipitation in *UP*, then this
240 could produce the near-concurrent deposition of sediments and ice that would be required
241 (discussed below) to form decametre thick and ice-rich sediments observed putatively in our
242 study region.

243 **5. The origin of excess ice to depth on Earth**

244 On Earth, alases form and are observed in conjunction with small-sized thermal-
245 contraction polygons and polygon-junction pits only where the permafrost (“ground that has
246 been frozen for at least two years”, Harris et al., 1988) is characterised by three conditions.
247 First, the permafrost must be “frost susceptible,” that is to say, composed of relatively fine-
248 grained sediments with small interstices; this enables and facilitates the migration of liquid
249 water through soil pores via cryosuction to a freezing front where ice lensing or “ice-
250 segregation” occurs (Harris et al., 1988; French, 2007; also, Hohmann, 1997). Second, the
251 permafrost must comprise “ground ice” (“frozen water presented as lenses, wedges, sheets,
252 seams or irregular masses”) that is “ice-rich”, also referred to as “excess ice” (Harris et al.,
253 1988). Third, the “excess ice” must have undergone thermal destabilisation. Typically, this
254 occurs in response to local or regional rises of sub-aerial temperatures (Washburn, 1973;
255 French, 2007). To form an alas, the thermal destabilisation engenders thaw, the volumetric
256 loss of meltwater by evaporation or drainage, and settling (or subsidence) of the previously
257 frozen sediments to a new equilibrium-depth below the original reference/surface datum
258 (Washburn, 1973; Harris et al., 1988; French, 2007).

259 The minimum depth of the ice-rich permafrost in which alases form can be
260 approximated by means of a rough calculation, assuming that all of the excess ice to the full
261 depth of the alas has been lost. For example, if an alas is ~80m deep and the ice-volume of
262 the permafrost in which it has formed is 50%, then the estimated depth of the ice-rich
263 permafrost prior to its destabilisation would be ~160m; this represents the initial volumetric
264 state of the ice-rich permafrost prior to being thawed (adapted from French, 2007).

265 Some of the depressions in our study region show depths approaching one hundred
266 metres (Costard and Kargel, 1995; Morgenstern et al., 2007; Soare et al., 2007; Séjourné et
267 al., 2011). If the Earth “alas” analogue is valid, then this depth could be indicative of excess
268 ice that is at least this deep if not deeper still. Were this so, a key question that remains
269 unanswered is the means by which excess ice that is 100m or deeper could have formed here.

270 **6. Ice-enrichment and the formation of deep “excess ice”**

271 **6.1 Freeze-thaw cycling, volcanic terrain and excess ice in the Kamchatka Peninsula,** 272 **Russia**

273 The Kamchatka peninsula in eastern Russia (~56°N) hosts thirty-six volcanoes that
274 are classified as 'active' (Kamchatka Volcanic Eruption Response Team (KVERT)
275 (<http://www.kscnet.ru>)). Seven of these volcanoes exhibit elevations in excess of ~3000m
276 above sea level. Mean (annual) temperatures are below 0°C and permafrost depths reach
277 ~1km at some locations (Sone et al., 2006; Abramov et al., 2008). Mean (annual)
278 precipitation of ~1000mm, punctuated by cold winters and mild summers, engenders
279 abundant freeze-thaw cycling and the formation of a disparate suite of meltwater-associated,
280 periglacial-landforms: small-sized (\leq ~30m in diameter) sorted and unsorted polygons (**Fig.**
281 **6**); ice wedges beneath polygon margins and junctures; earth hummocks; solifluction lobes;
282 and needle ice (Sone et al., 2006; Abramov et al., 2008).

283 Many of these landforms are rooted in the regional (basaltic) volcanic-plateaus and

284 plains that have formed as the result of fissure eruptions, the most recent of which occurred in
285 1975 and 1976 (Abramov et al., 2008). These plateaus and plains are comprised of basaltic
286 lavas, as well as ashes and cinders; these relatively fine-grained volcanoclastic sediments
287 facilitate the formation of excess ice if and when meltwater is available and freeze-thaw
288 cycling takes place. Moreover, the relatively low thermal-conductivity of volcanic sediments
289 permits buried or even near-surface ground ice to persist and survive even when new (and
290 possibly hot) volcanic deposits accumulate at the surface (Sone et al., 2006; Abramov et al.,
291 2008).

292 Abramov *et al.* (2008) investigated thirteen borehole sites in this region, the deepest
293 of which is ~25m; ground ice comprised ~20-80% of the extracted material by weight.
294 Multiple borehole-samples exhibited discrete near-surface ice wedges embedded
295 epigenetically in the volcanic cinders and scoria produced by the fissure eruptions of 1975
296 and 1976 (Abramov et al., 2008). Lenses of massive ice (beds or layers essentially of pure
297 ice) were observed deep within the soil column and were overlain by metre and sub-metre
298 horizons of volcanic ash, basalt, sand and/or ice (possibly firnified buried-snow) (Abramov et
299 al., 2008).

300 The intermittent presence of ice-rich permafrost to depth within the soil column was
301 observed at most of the borehole sites; the importance of this is two-fold. First, it points to
302 multiple episodes of ice enrichment, by means of seasonally or volcanically-induced freeze-
303 thaw cycling, alternating with multiple episodes of volcanism; second, it highlights the low
304 thermal-conductivity of volcanic material, as the ice-rich structures at depth are preserved
305 beneath metres of volcanically-derived and subsequently-accumulated sediments that may
306 have been hot at the time of deposition.

307 **6.2 Possible freeze-thaw cycling, volcanic terrain and putative excess ice in Utopia**

308 **Planitia**

309 Having used the *HiRISE*, *OMEGA*, and *CRISM* data to evaluate the physical and
310 spectral properties of the dark-toned terrain in our study region, we propose that the terrain is
311 comprised of relatively fine-grained sediments; we hypothesise that the terrain could be the
312 indirect depositional product of explosive volcanism. Furthermore, we suggest that the
313 presence of the scalloped depressions, small-sized polygons and polygon junction-pits is a
314 marker of ice-rich terrain, minimally, to decametres of depth. Writ large, our dark-toned
315 terrain formation-hypothesis comprises three key stages (**Fig. 7**).

316 **Stage 1: Sediment deposition**

317 Explosive volcanic-events (either singular or episodic and discrete) in Alba Mons,
318 Syrtis Major or Arabia Terra, generate volcanic ash that is deposited by air-fall in our study
319 region. Over time this creates thick (possibly decametres or more) deposits of dark-toned
320 sediments. At high spatial-resolution, the dark-toned terrain exhibits sub-metre boulders and
321 drifts of dark wind-blown sediment (**Fig. 3**). These drifts rarely coalesce into aeolian
322 bedforms, suggesting (but not necessarily requiring) that the grain size of the sediments
323 generally is smaller than sand (Bagnold, 1941). This is consistent with the grain size of
324 volcanic ash and, as observed in the Kamchatka peninsula, is an ideal sedimentary-medium
325 for the development of ground ice because of its high porosity and “frost susceptibility” (high
326 potential for cryosuction) (French, 2007; also, Hohmann, 1997).

327 **Stage 2: Snow/ice deposition**

328 Under current boundary-conditions the precipitation and deposition of water ice/frost
329 is seasonal, ephemeral and constrained by latitude; near the northern Martian pole water
330 ice/frost accumulates on the ground during the winter and sublimates in response to rising
331 temperatures in the spring (Appéré et al., 2011). However, numerous researchers suggest that
332 recent higher-obliquities could have engendered north polar ice-cap sublimation and
333 significant global rises of atmospheric water-vapour, temperature and pressure (e.g. Head et

334 al., 2003; Forget et al., 2006; Madeleine et al., 2009, 2014). At lower latitudes, this could
335 have been marked by substantial increases in the atmospheric condensation and precipitation
336 of water-ice/snow and its accumulation on the ground, so much so that large-scale ice sheets
337 comprising kilometres of depth would have formed (e.g. Head et al., 2003; Forget et al.,
338 2006; Madeleine et al., 2009, 2014).

339 Recently, Halevy and Head (2014) have hypothesised that early Mars sustained
340 intermittently-warm (at and above 0⁰C) boundary conditions as the result of strong albeit
341 brief episodes of volcanic eruptions and the associated discharge/rise of atmospheric
342 greenhouse-gases. This would have generated transiently-higher atmospheric (H₂O) vapour-
343 pressures, as surface deposits of ice and snow evaporate or sublimate, as well as enhanced
344 rates of precipitation when the water-vapour condenses (Halevy and Head, 2014). We suggest
345 that a similar procession of events, derived of explosive volcanism, could have generated
346 local melt-tolerant conditions in the late Amazonian Epoch at the mid-latitudes of *UP*.

347 **Stage 3: Freeze/thaw cycling**

348 Ground ice, let alone excess ice, begins to form as snow or ice at or near the surface
349 melts, migrates into the underlying fine-grained and frost-susceptible terrain and then freezes
350 in *situ*. The build-up of excess ice during freezing is driven by the difference in chemical
351 potential between freezing ice and liquid water driving water toward a freezing front(s) (Dash
352 et al., 2006); iterations of this process create epigenetic ice-lenses, wedges, seams or
353 irregular-masses, much as it has in the ice-rich volcanic terrain of the Klyuchevskoy National
354 Park.

355 We propose that the ice-enrichment of the (decametre-deep) dark-toned terrain at the
356 mid-latitudes of *UP* occurred episodically and cyclically: discrete layers of fine-grained and
357 volcanically-derived ash accumulated alternately with discrete layers of snow and/or ice. This
358 assumption is consistent with the possible stratification observed in some scalloped

359 depressions (**Fig. 5**). Moreover, and as noted above, the relatively low-thermal conductivity
360 of ash or other volcanic sediments would enable surface, near-surface or buried snow or ice
361 to persist and survive even when new deposits of these sediments accumulate at the surface.

362 Extended periods of alternating deposition, accumulation and thaw-freeze cycling
363 could produce horizons or layers of ice-rich volcanic terrain metres to possibly hundreds of
364 metres deep, even if the individual and alternating layers of ash and snow or ice are relatively
365 thin. In addition to our proposed analogue site at Kamchatka, this scenario is also akin to the
366 emplacement and formation of (perennial and persistent) niveo-aeolian deposits of sand and
367 snow in the McMurdo Dry Valleys, Antarctica (Cailleux, 1972; Heldmann et al., 2012), and
368 of (annual and ephemeral) deposits of sand or silt and snow layers at Poste-de-la-Baleine,
369 Quebec, Canada (Cailleux, 1972).

370 Cyclical excursions above and below 0°C do not require aerial and sub-aerial
371 boundary conditions that are radically different from current ones. Even under current
372 conditions on Mars, liquid water is thought to be meta-stable where thin ice is sheltered
373 locally in small depressions and gully alcoves and is illuminated by normal-incidence
374 insolation (Hecht, 2002; also see e.g. Levy et al., 2009c; Schon and Head, 2011, 2012). If the
375 presence of surface and near-surface ground ice is integrated with estimates of Martian
376 degree days (above 0°C and below the boiling point of water), then “favourable” regions
377 where water could currently be stable locally comprise 29% of the Martian surface (Haberle
378 et al., 2001). Punctuated by the type of volcanic activity discussed by Halevy and Head
379 (2014) or hypothesised by us, these favourable conditions could have been in place
380 throughout the period when the decametres-deep excess-ice formed in *UP*.

381 **7. Alternate formation hypotheses**

382 **7.1.Vapour diffusion and condensation**

383 **7.1.1.: Vapour diffusion and condensation: a model**

384 Although the possible meta-stability of highly-localised pockets of water on Mars
385 today is acknowledged by many researchers, very few of them believe that liquid water is/has
386 been stable at the mid-latitudes of *UP* for a period of time sufficient to form the scalloped
387 depressions by means of melting and evaporation (Mellon and Jakosky, 1993, 1995;
388 Shorghofer and Aharonson, 2005; Hudson et al., 2009; Shorghofer and Forget, 2012). Thus,
389 if the depressions are alases that evolved in an ice-rich medium, possibly excess ice, then the
390 origin of the excess ice could only be explained by means of atmospheric diffusion and
391 adsorption/condensation (e.g. Morgenstern et al., 2007; Lefort et al., 2009).

392 Multiple models of (global) atmospheric circulation suggest that the sublimation of
393 the perennial polar-caps and the derived (global) abundance of atmospheric water-vapour
394 vary in response to changes of Mars spin axis and eccentricity (e.g. Mellon and Jakosky,
395 1993, 1995; Head et al., 2003; Madeleine et al., 2009, 2014). For example, higher obliquities
396 could induce increased polar-sublimation and, in so doing, enhance the global abundance of
397 atmospheric water-vapour. This would facilitate the diffusion, saturation, and condensation of
398 water vapour (as ground ice) within the interstices or pore space of near-surface regolith at
399 non-polar latitudes.

400 Some diffusion and condensation models show that during periods of high obliquity
401 seasonal thermal-oscillations at the mid-latitudes could drive water vapour into the pore space
402 of near-surface regolith, forming ground ice to as much as ten metres of depth (Mellon and
403 Jakosky, 1993, 1995); however, the oscillations would be too weak to fill all of the available
404 pore space and excess ice could not form, even close to the surface (Mellon and Jakosky,
405 1995).

406 The inability of the oscillations to form excess ice largely is the result of three
407 variables: (a) the shortness of time and of depth/intensity that characterises thermal
408 oscillation driven by seasonality; (b) to the extent that the upper few metres of regolith

409 approach ice saturation more quickly than the metres at a greater depth, this forms a diffusive
410 barrier that chokes the further transport of vapour to depth; and to a lesser degree, (c) the
411 geothermal gradient, whose temperature raises the required density of vapour-saturation
412 beyond that which can be achieved by condensation at $\geq 10\text{m}$ (Mellon and Jakosky, 1995).
413 Deeper ground ice, let alone the possibility of excess ice, is explained by ice having been
414 buried antecedent to the most recent changes of orbital parameters or by the upward transport
415 and freezing of vapour derived of a deep ground-water table (Mellon and Jakosky, 1995)

416 More recently, Fisher and Lacelle (2014, also see Fisher, 2005) have used data and
417 observations associated with the Phoenix Lander site to suggest that the penetration depth of
418 thermal contraction-cracking can facilitate the transport and concentration of water vapour to
419 a few metres of depth, sufficiently so to form excess ice. Excess-ice that possibly comprises
420 decametres of depth, however, is not considered.

421 **7.1.2 Excess ice formation by vapour diffusion and condensation on Earth**

422 The McMurdo Dry Valleys of the Antarctic exhibit sub-zero temperatures and hyper-
423 aridity similar enough to Mars for this polar region to serve as a possible Mars
424 (climatological) analogue (Marchant et al., 2002; Levy et al., 2009c; Lacelle et al., 2011,
425 2013; Marinova et al., 2011; 2013). Interestingly, at various locations within the Dry Valleys
426 ice-rich permafrost has been identified but only within a metre or so of the surface (French
427 and Guglielman, 2000; Bockheim and Hall, 2002; Lacelle et al., 2011, 2013; Marinova et al.,
428 2011; 2013). This near-surface ground (sometimes excess) ice is thought to have formed
429 epigenetically, under the temperature regimes and rises associated with inter-glacial/glacial
430 periods, and by means of vapour-diffusion and condensation (Lacelle et al., 2011; also,
431 Marchant et al., 2002; Lacelle et al., 2013; Marinova et al., 2011, 2013).

432 **7.2 Ice-dust mantle degradation**

433 Some researchers propose that the spatially-associated suite of *PPLs* at the mid-

434 latitudes of *UP* comprises the degradational remnants of a light-toned and region-wide ice-
435 dust mantle (e.g. Tanaka et al., 2005; Morgenstern et al., 2007; Lefort et al., 2009; Levy et
436 al., 2009a-c, 2010; Ulrich et al., 2010). This mantle is thought to have formed by means of
437 atmospheric precipitation during the very late Amazonian Epoch, under the meteorological
438 influence of changes in the spin axis and/or its orbital eccentricity of Mars (Head et al., 2003;
439 Madeleine et al., 2009, 2014).

440 Our recent work (Soare et al., 2012a), in line with the observations reported above,
441 shows that the *PPLs* in our study region incise terrain that is dark-toned, not light-toned
442 (**Figs. 2-3**); we also noted that wherever the dark and light-toned terrains are observed
443 together, the dark-toned terrain either underlies the light-toned terrain or it resides at a lower
444 elevation (Soare et al., 2012a). Consequently, the light-toned terrain post-dates the dark-toned
445 terrain, could not be its geological (degradational) precursor and cannot comprise the
446 periglacial medium out of which the scalloped depressions and the two other *PPLs* have
447 formed. Thus, although the light-toned mantle may contain ice, long-term periglacial
448 modification processes appear to be concentrated in the underlying and older dark terrain.

449 **8. Discussion and conclusion**

450 Agreement is widespread within the community of Mars researchers that the
451 scalloped depressions and the spatially-associated *PPLs* are indicative of ice-rich terrain that
452 is tens of decametres deep (e.g. Costard and Kargel, 1995; Morgenstern et al., 2007; Soare et
453 al., 2007, 2008; Lefort et al., 2009; Séjourné et al., 2011). On the other hand, except for the
454 work of a few researchers (Morgenstern et al., 2007; Séjourné et al., 2012; Soare et al., 2012),
455 robust discussions of region-wide processes, lithologies, and cryostratigraphies required to
456 induce ice enrichment to decametres of depth is unapparent in the literature.

457 Previous studies have shown that many regions covered in dark-toned surface
458 sediments elsewhere in the northern plains are consistent with weathered iron-bearing glass

459 (Horgan and Bell, 2012). In this study, we have used the *OMEGA* and *CRISM* data in mid-
460 *UP* to show that the spectral properties of the dark-toned terrain incised by the scalloped
461 depressions and two other *PPLs* are spectrally consistent with weathered glass-rich basalt,
462 similar to weathered volcanic tephra on Mauna Kea. We also draw upon the dark-toned and
463 volcanic terrain in Kamchatka as an analogical foundation for three assumptions about the
464 possible formation of ice-rich terrain in our study region.

465 First, sediments similar in composition and origin to those deposited around the
466 Kamchatkan volcanoes could have been delivered, deposited and accumulated to depth
467 (perhaps episodically) in mid-*UP*, probably by air fall, as the result of explosive volcanism.
468 Intertwined with this air-fall deposition of volcanic material would be the seasonal (under the
469 influence of disparate orbital eccentricities and/or obliquities) or volcanically-induced (by
470 means of enhanced higher temperatures and enhanced water-vapour abundances in the
471 atmosphere) deposition of snow or ice.

472 Second, on Mars as on Earth the permeability and porosity of volcanically-derived
473 sediments make them an ideal medium for the infiltration and subsequent (epigenetic)
474 freezing of meltwater, but only in as much as appropriate triple-point conditions are in place.
475 Recent work by a number of researchers points to explosive volcanism possibly having
476 generated aerial and sub-aerial boundary conditions in mid-*UP* during the late Amazonian
477 Epoch that are at least transiently consistent with the freeze-thaw cycling of surface and near-
478 surface water-ice or snow.

479 Third, the relatively low thermal-conductivity of volcanic sediments facilitates the
480 preservation or survival of ground ice at depth, even when it undergoes burial by fresh and
481 potentially hot volcanic-sediments that are deposited subsequent to the formation of that
482 ground ice. We suggest that the dark-toned terrain incised by the *PPLs* and scalloped
483 depressions is ice-rich to depth and that its ice-enrichment is the work of snow/ice surface

484 deposits that have undergone freeze-thaw cycling and burial.

485 We cannot rule out atmospheric diffusion and vapour condensation as the process by
486 which ground ice forms in the near-surface regolith of our study region, but the leading
487 vapour diffusion/condensation models and hypotheses do not account for the formation of
488 excess ice to decametres of depth on Mars. Moreover, in as much as there are no observed
489 field-sites on Earth where decametres-deep excess ice has been formed by vapour diffusion
490 and condensation, the empirical validation of the diffusion and condensation models and
491 hypotheses awaits further work.

492 **Acknowledgments**

493 We would like to thank an anonymous reviewer for helpful comments, questions, and advice.
494 SJC is funded by a Leverhulme Trust Grant RPG-397 and by a research grant channeled
495 through RJS. M.R.EL-M is funded by the Swiss National Science Foundation (SNF).

496 **References**

- 497 Abramov, A., Gruber, S., Gilchinsky, D., 2008. Mountain permafrost on active volcanoes:
498 Field data and statistical mapping; Klyuchevskaya volcano group, Kamchatka, Russia.
499 Permafrost and Periglacial Processes 19: 261-277, doi:10.1002/ppp.622.
- 500 Adams, J.B., 1968. Lunar and Martian surfaces: petrologic significance of absorption bands
501 in the near-infrared. Science 159, 3, 1453-1455, doi:10.1126/science.159.3822.1453.
- 502 Arnalds, O., Gisladottir, F.O., Sigurjonsson, H., 2001. Sandy deserts of Iceland: an overview.
503 Journal of Arid Environments 47, 3, 359-371, doi:10.1006/jare.2000.0680.
- 504 Bagnold, R.A., 1941. The physics of wind-blown sand and desert dunes. Methuen, London
505 265 p.
- 506 Bibring, J.P. et al., 2005. Mars surface diversity as revealed by the OMEGA/Mars Express
507 observations. Science 307, 5, 1576-1581, doi:10.1126/science.1108806.
- 508 Bockheim, J.G., Hall, K.J., 2002. Permafrost, active-layer dynamics and periglacial

- 509 environments of continental Antarctica. *South African Journal of Science* 98, 82-90.
- 510 Cailleux, A., 1972. Les formes et dépôts nivéo-éoliens actuels en Antarctique et au Nouveau
511 Québec. *Cahiers de géographie du Québec* 16, 39, 377-409.
- 512 Costard, F.M., Kargel, J.S., 1995. Outwash plains and thermokarst on Mars. *Icarus* 114, 1,
513 93-112, doi:10.1006/icar.1995.1046.
- 514 Dash, J.G., Rempel, A.W., Wettlaufer, J.S., 2006. The physics of pre-melted ice and its
515 geophysical consequences. *Reviews of Modern Physics* 78, 695–741, doi:10.1103/
516 RevModPhys.78.695.
- 517 Fischer, E.M., Pieters, C.M., 1993. The continuum slope of Mars: bidirectional reflectance
518 investigations and applications to Olympus Mons. *Icarus* 102, 2, 185-202, doi:10.
519 1006/icar.1993.1043.
- 520 Fisher, D.A., 2005., A process to make massive ice in the martian regolith using long term
521 diffusion and thermal cracking. *Icarus* 179, 387-397, doi:10.1016/j.icarus.2005.07.
522 024.
- 523 Fisher, D.A., Lacelle, D., 2014. A model for co-isotopic signatures of evolving ground ice in
524 the cold dry environments of Earth and Mars. *Icarus* 243, 454-470,
525 doi.org/10.1016/j.icarus.2014.08.009.
- 526 Forget, F., Haberle, R.M., Montmessin, F, Levrard, B., Head, J.W., 2006. Formation of
527 glaciers on Mars by atmospheric precipitation at high obliquity. *Science* 311, 368-
528 371, doi:10/1126.science.1120335.
- 529 French, H.M., 2007. *The periglacial environment*, 3rd ed., J. Wiley & Sons, West Sussex,
530 England, 458 p.
- 531 French, H.M., Gulgielman, M., 2000. Frozen ground phenomena in the vicinity of Terra
532 Nova Bay, Northern Victoria Land, Antarctica: a preliminary report. *Geografiska*
533 *Annaler* 82A, 513-526.

- 534 Haberle, R.M., McKay, C.P., Schaeffer, J., Cabrol., N.A., Grin. E.A., Zent, A.P., Quinn, R.,
535 2001. On the possibility of liquid water on present-day Mars. *Journal of Geophysical*
536 *Research* 106, E10, 23,317-326.
- 537 Halevy, I., Head, J.W., 2014. Episodic warming of early Mars by punctuated volcanism.
538 *Nature Geoscience* 7, 865–868, doi:10.1038/ngeo2293.
- 539 Harris, S.A, French, H.M., Heginbottom, J.A., Johnston, G.H., Ladanyi, B., Sege, D.C., van
540 Everdingen, R.O., (eds.), 1988. Glossary of permafrost and related ground-ice terms.
541 Technical Memorandum 142, Permafrost Subcommittee, National Research Council
542 of Canada.
- 543 Hauber et al., 2011. Periglacial landscapes on Svalbard: Terrestrial analogs for cold-climate
544 landforms on Mars, in Garry. W.B., and Bleacher, J.E., eds., *Analogues for planetary*
545 *exploration: Geological Society of America Special Paper* 483, 177-201, doi:10.1130/
546 2011.2483(12).
- 547 Head, J.W., Mustard, J.F., Kreslavsky, M.A., Milliken, R.E., Marchant, D.R., 2003. Recent
548 ice ages on Mars. *Nature* 426, 797-802, doi:10.1038/nature02114.
- 549 Hecht, M.H., 2002. Metastability of liquid water on Mars. *Icarus* 156, 373-386, doi:10.1006/
550 icar.2001.6794.
- 551 Heldmann, J.L., Marinova, M., Williams, K.E., Lacelle, D., McKay, C.P., Davila, A., Pollard,
552 W., Andersen, D.T., 2012. Formation and evolution of buried snowpack deposits in
553 Pearse Valley, Antarctica, and implications for Mars. *Antarctic Science* 24, 3 299-
554 316, doi:10.1017/S095410 2011000903.
- 555 Hohmann, M., 1997. Soil freezing-the concept of soil water potential. State of the art. *Cold*
556 *regions Science and Technology* 25, 101-110.
- 557 Horgan, B., Bell, J.F., 2012. Widespread weathered glass on the surface of Mars. *Geology*
558 40, 391-394, doi:10.1130/G32755.1.

- 559 Horgan, B., Smith, R., Mann, P., Stromberg, J., 2013. New evidence for a weathering
560 origin for the high-silica component of TES surface type 2 on Mars. 44th Lunar and
561 Planetary Science Conference, 3032.
- 562 Horgan, B., Cloutis, E.A., Mann, P., Bell, J.F., 2014. Near-infrared spectra of ferrous mineral
563 mixtures and methods for their identification in planetary surface spectra. *Icarus* 234,
564 132-154, doi:10.1016/j.icarus.2014.02.031.
- 565 Hudson, T.L., Aharonson, O., Schorghofer, N., 2009. Laboratory experiments and models
566 of diffusive emplacement of ground ice on Mars. *Journal of Geophysical Research*
567 114, E01002, doi:10.1029/2008JE003149.
- 568 Kerber, L., Head, J.W., Madeleine, J.B., Forget, F., Wilson, L., 2012. The dispersal of
569 pyroclasts from ancient explosive volcanoes on Mars: implications for friable layered
570 deposits. *Icarus* 219, 358–381, doi:10.1016/j.icarus.2012.03.016.
- 571 Kraft, M.D., Sharp, T.G., Michalski, J.R., Rampe, E.B., 2007. Combined thermal and near-
572 infrared spectra of hydrous silica coatings: implications for surface type 2 mineralogy
573 and recent liquid water on Mars. 38th Lunar and Planetary Science Conference, 2241.
- 574 Lacelle, D. et al., 2011. Vapor-diffusion origin (condensation-adsorption) in ice cemented
575 permafrost spanning the last 135,5 Ka years in University Valley, Dry Valleys of
576 Antarctica. 5th Mars Polar Conference, 6083.
- 577 Lacelle, D., Fisher, D., Clark, I.D., Berinstain, A., 2008. Distinguishing between vapor- and
578 liquid-formed ground ice in the northern martian regolith and potential for
579 biosignatures preserved in ice bodies. *Icarus* 197, 458-469, doi:10.1016/j.icarus.2008.
580 05.017.
- 581 Lefort, A., Russell, P.W., McEwen, A.S., Dundas, C.M., Kirk, R.L., 2009. Observations of
582 periglacial landforms in Utopia Planitia with the High Resolution Imaging Science
583 Experiment (HiRISE). *Journal of Geophysical Research* 114, E04005, doi:10.1029/

- 584 2008JE003264.
- 585 Levy, J., Head, J.W, Marchant, D.R., 2009a. Thermal contraction crack polygons on Mars:
586 Classification, distribution and climatic implications from HiRISE observations.
587 Journal of Geophysical Research 114, E01007, doi:10.1029/2008JE003273.
- 588 Levy, J., Head, J.W, Marchant, D.R., 2009b. Concentric crater fill in Utopia Planitia: History
589 and interaction between glacial “brain terrain” and periglacial mantle processes.
590 Icarus 202, 462-476, doi:10.1016/j.icarus.2009.02.018.
- 591 Levy, J.S., Head., J.W., Marchant, D.R., Dickson, J.L., Morgan, G.A., 2009c. Geologically
592 recent gully-polygon relationships on Mars: insights from the Antarctic Dry Valleys
593 on the roles of permafrost, microclimates, and water sources for surface flow. Icarus
594 201, 113-126, doi:10.1016/j.icarus.2008.12.043.
- 595 Levy, J.S., Head, J.W., Marchant, D.R., 2010. Thermal contraction crack polygons on Mars:
596 A synthesis from HiRISE, Phoenix, and terrestrial analog studies. Icarus 206, 229-
597 252, doi:10.1016/j.icarus.2009.09.005.
- 598 Lorenz, R.D., 2000. Microtektites on Mars: volume and texture of distal impact ejecta
599 deposits. Icarus 144, 2, 353-366, doi:10.1006/icar.1999.1603.
- 600 Madeleine, J.B., Forget, F., Head, J.W., Levrard, B., Montmessin, F., Millour, E., 2009.
601 Amazonian northern mid-latitude glaciation on Mars: a proposed climate scenario.
602 Icarus 203, 390-405, doi:10.1016/j.icarus.2009.04.037.
- 603 Madeleine, J.B., et al., 2014. Recent Ice Ages on Mars: the role of radiatively active clouds
604 and cloud microphysics. Geophysical Research Letters 41, 1-7; doi:10.1002/2014GL
605 O59861
- 606 Malin, M.C., Edgett, K.S., 2001. Mars Global Surveyor Mars Orbiter Camera: interplanetary
607 cruise through primary mission. Journal of Geophysical Research 106, E10, 23429-
608 23570, doi:10.1029/2000JE001455.

- 609 Marinova, M.M., et al., 2013. Distribution of depth to ice-cemented soils in the high-
610 elevation Quartermain Mountains, McMurdo Dry Valleys, Antarctica. *Antarctic*
611 *Science* 25, 4, 575-582, doi:10.1017/S095410201200123X.
- 612 Marinova, M.M et al., 2011. The high-elevation Dry Valleys of Antarctica as a Mars Polar
613 Analogue: mapping subsurface ice distribution and modeling its stability. 5th Mars
614 Polar Conference, 6051.
- 615 McEwen, A.S., et al., 2007. Mars Reconnaissance Orbiter's High Resolution Imaging Science
616 Experiment (HiRISE). *Journal of Geophysical Research* 112, E5, doi:10.1029/2005JE
617 002605.
- 618 Mellon, M.T., Jakosky, B.M., 1993. Geographic variations in the thermal and diffusive
619 stability of ground ice on Mars. *Journal of Geophysical Research* 98, E2, 3345-3364.
- 620 Mellon, M.T., Jakosky, B.M., 1995. The distribution and behavior of Martian ground ice
621 during past and present epochs. *Journal of Geophysical Research* 100, E6, 11,781-
622 11,799.
- 623 Mellon, M.T., 1997. Small-scale polygon features on Mars: Seasonal thermal contraction
624 cracks in permafrost. *Journal of Geophysical Research* 102, E11, 25,617-25,628.
- 625 Michalski, J.R., Bleacher, J.E., 2013. Supervolcanoes within an ancient volcanic province in
626 Arabia Terra, Mars. *Nature* 502, 7, 47-52, doi:10.1038/nature12482.
- 627 Milliken, R.E., Mustard, J.F., Goldsby, D.L., 2003. Viscous flow features on the surface of
628 Mars: Observations from high-resolution Mars Orbiter Camera (MOC) images.
629 *Journal of Geophysical Research* 108, E6, 5057, doi:10.1029/2002JE002005.
- 630 Milliken, R. et al., 2008. Opaline silica in young deposits on Mars. *Geology* 36, 11, 847,
631 doi:10.1130/G24967A.1.
- 632 Minitti, M., Weitz, C.M, Lane, M.D., Bishop, J.L, 2007. Morphology, chemistry, and spectral

- 633 properties of Hawaiian rock coatings and implications for Mars. *Journal of*
634 *Geophysical Research* 112, E5, doi:10.1029/2006JE002839.
- 635 Morgenstern, A., Hauber, E., Reiss, D., van Gasselt, S., Grosse, G., Schirrmeyer, L., 2007.
636 Deposition and degradation of a volatile-rich layer in Utopia Planitia, and
637 implications for climate history on Mars. *Journal of Geophysical Research* 112,
638 E06010, doi:10.1029/2006JE002869.
- 639 Murchie, S. et al., 2007. Compact Reconnaissance Imaging Spectrometer for Mars (CRISM)
640 on Mars Reconnaissance Orbiter (MRO). *Journal of Geophysical Research* 112, E5,
641 doi:10.1029/2006JE002682.
- 642 Mustard, J.F., Cooper, C.D., Rifkin, M.R., 2001. Evidence for recent climate change on Mars
643 from the identification of youthful near-surface ground ice. *Nature* 412, 411-414.
644 doi:10.1038/35086515.
- 645 Mustard, J.F., Poulet, F., Gendrin, A., Bibring, J.P., Langevin, Y., Gondet, B., Mangold, N.,
646 Bellucci, G., Altieri, F., 2005. Olivine and pyroxene diversity in the crust of Mars.
647 *Science* 307, 1594, doi:10.1126/science.1109098.
- 648 Ody, A., Poulet, F., Langevin, Y., Bibring, J.P., Bellucci, G., Altieri, F., Gondet, B.,
649 Vincendon, M., Carter, J., Manaud, N., 2012. Global maps of anhydrous minerals at
650 the surface of Mars from OMEGA/MEx. *Journal of Geophysical Research* 117,
651 E00J14, doi:10.1029/2012JE004117.
- 652 Poulet, F., Langevin, Y., Boubin, G., Jouglet, D., Bibring, J-P., Gondet, B., 2008. Spectral
653 variability of the Martian high latitude surfaces. *Geophysical Research Letters*. 35, 2,
654 20201, doi:10.1029/2008GL035450.
- 655 Salvatore, M.R., Mustard, J.F., Wyatt, M.B., Murchie, S.L., 2010. Definitive evidence of
656 Hesperian basalt in Acidalia and Chryse Planitiae. *Journal of Geophysical Research*
657 115, E7, doi:10.1029/2009JE003519.

- 658 Salvatore, M.R., Mustard, J.F., Head, J.W., Cooper, R.F., Marchant, D.R., Wyatt, M.B.,
659 2013. Development of alteration rinds by oxidative weathering processes in Beacon
660 Valley, Antarctica, and implications for Mars. *Geochimica et Cosmochimica Acta*.
661 115, 137-161, doi:10.1016/j.gca.2013.04.002.
- 662 Schon, S.C., Head, J.W., 2011. Keys to gully formation processes on Mars: relation to
663 climate cycles and sources of meltwater. *Icarus* 213, 428-432, [doi:10.1016/j.icarus.](https://doi.org/10.1016/j.icarus.2011.02.020)
664 [2011.02.020](https://doi.org/10.1016/j.icarus.2011.02.020).
- 665 Schon, S.C., Head, J.W., 2012. Gasa impact crater, Mars: very young gullies formed from
666 impact into latitude-dependent mantle and debris-covered glacier deposits. *Icarus* 218,
667 459-477, doi:10.1016/j.icarus.2012.01.002.
- 668 Schultz, P.H., Mustard, J.F., 2004. Impact melts and glasses on Mars. *Journal of Geophysical*
669 *Research* 109, E1, doi:10.1029/2002JE002025.
- 670 Seelos, F.P., Murchie, S.L., Humm, D.C., Barnouin, O.S., Morgan, F., Taylor, H.W., Hash,
671 C. and team., 2011. CRISM data processing and analysis products update -
672 calibration, correction, and visualization, 42nd Lunar and Planetary Science
673 Conference, 1438.
- 674 Seelos, K.D., Arvidson, R.E., Jolliff, B.L., Chemtob, S.M., Morris, R.V., Ming, D.W.,
675 Swayze, G.A., 2010. Silica in a Mars analog environment: Ka'u Desert, Kilauea
676 Volcano, Hawaii. *Journal of Geophysical Research*, 115, E4, doi:10.1029/2009JE00
677 3347.
- 678 Seelos, K.D., Seelos, F.P., Viviano-Beck, C.E., Murchie, S.L., Arvidson, R.E., Ehlmann,
679 B.L., Fraeman, A.A., 2014. Mineralogy of the MSL Curiosity landing site in Gale
680 crater as observed by MRO/CRISM. *Geophysical Research Letters* 41, 14, 48804887,
681 doi:10.1002/2014GL060310.
- 682 Seibert, N.M., Kargel, J.S., 2001. Small-scale Martian polygonal terrain: implications for

- 683 liquid surface water. *Geophysical Research Letters* 28, 899-902.
- 684 Séjourné, A., Costard, F., Gargani, J., Soare, R.J., Marmo, C., 2010. The polygon junction pits
685 as evidence of a particularly ice-rich area in Utopia Planitia. 40th Lunar and Planetary
686 Science Conference, 2113.
- 687 Séjourné, A., Costard, F., Gargani, J., Soare, R.J., Fedorov, A., Marmo, C., 2011. Scalloped
688 depressions and small-sized polygons in western Utopia Planitia: a new formation
689 hypothesis. *Planetary and Space Science* 59, 412-422, doi:10.1016/j.pss.2011.01.007.
- 690 Séjourné, A., Costard, F.N., Gargani, J., Soare, R.J., Marmo, C., 2012. Evidence of an
691 eolian ice-rich and stratified permafrost in Utopia Planitia, Mars. *Planetary and Space
692 Science* 60, 348-254, doi:10.1016/j.pss.2011.09.004.
- 693 Shorghofer, N., Aharonson, O., 2005. Stability and exchange of subsurface ice on Mars.
694 *Geophysical Research Letters* 110, E05003. doi:10.1029/2004JE002350.
- 695 Shorghofer, N., 2007. Dynamics of ice ages on Mars. *Nature* 449, 192-195, doi:10.1038/
696 nature06082.
- 697 Shorghofer, N., and Forget, F., 2012. History and anatomy of subsurface ice on Mars. *Icarus*
698 220, 2, 1112-1120, doi:10.1016/j.icarus.2012.07.003.
- 699 Singer, R. B., 1982. Spectral evidence for the mineralogy of high-albedo soils and dust on
700 Mars, *International Colloquium on Mars*, 87, 10159-10168, doi:10.1029/JB087iB12p
701 10159.
- 702 Soare, R.J., Kargel, J.S., Osinski, G.R., Costard, F., 2007. Thermokarst processes and the
703 origin of crater-wall gullies in Utopia and western Elysium Planitia. *Icarus* 1, 191,
704 195-212, doi:10.1016/j.icarus.2007.04.018.
- 705 Soare, R.J., Osinski, G.R., and Roehm, C.L., 2008. Thermokarst lakes and ponds on Mars
706 in the very recent (late Amazonian) past. *Earth and Planetary Science Letters* 272, 1-
707 2, 382-393, doi:10.1016/j.epsl.2008.05.10.

- 708 Soare, R.J., Osinski, G.R., 2009. Stratigraphical evidence of late Amazonian periglaciation
709 and glaciation in the Astapus Colles region of Mars. *Icarus* 202 (1) 17-21. doi:10.
710 1016/j.icarus.2009.02.009.
- 711 Soare, R.J., Séjourné, A., Pearce, G., Costard, F., Osinski, G.R., 2011. The Tuktoyaktuk
712 Coastlands of northern Canada: a possible “wet” periglacial analogue of Utopia
713 Planitia, Mars, in Garry, W.B., and Bleacher, J.E., eds., *Analogues for planetary
714 exploration: Geological Society of America Special Paper 483*, 203-218, doi:10.1130/
715 2011.2483(13).
- 716 Soare, R.J., Conway, S., Costard, F., Dohm, J.M., Séjourné, A., 2012a. Climate change
717 & the origin of ice-rich permafrost (segregation ice) in mid Utopia Planitia, Mars.
718 Mars Recent Climate Change Workshop. Moffett Field, California.
- 719 Soare, R.J., Costard, F.N., Pearce, G., Séjourné, A., 2012b. A re-interpretation of the recent
720 stratigraphical history of Utopia Planitia: implications for late-Amazonian periglacial
721 terrain and an ice-rich mantle. *Planetary and Space Science* 60, 131-139,
722 doi:10.1016/j.pss.2011.07.007.
- 723 Sone, T., Yamagata, K., Otsuki, Y., Sawada, Y., Vyatkina, M., 2006. Distribution of
724 permafrost on the west slope of Mt. Ichinsky, Kamchatka, Russia. *Bulletin of
725 Glaciological Research* 23. 69-75.
- 726 Souness, C.J., Abramov, A., 2012. The volcanic terrains of Kamchatka, eastern Russia: a
727 glacial and periglacial environment with potential for Mars analog-based research.
728 43rd Lunar and Planetary Science Conference, 1071.
- 729 Tanaka, K.L., Skinner, J.A., Hare, T.M., 2005. Geologic map of the northern plains of Mars,
730 scale 1:15,000,000. U.S. Geological Survey Scientific Investigation, Map 2888.
- 731 The Kamchatka Volcanic Eruption Response Team: [http://www.kscnet.ru/ivs/kvert/index_](http://www.kscnet.ru/ivs/kvert/index_eng.php)
732 [eng.php](http://www.kscnet.ru/ivs/kvert/index_eng.php).

- 733 Ulrich, M., Morgenstern, A., Günther, F., Reiss, R., Bauch, K.E., Hauber, E., Rössler, S.,
 734 Schirrmeister, L., 2010. Thermokarst in Siberian ice-rich permafrost: comparison to
 735 asymmetric scalloped depressions on Mars. *Journal of Geophysical Research* 115,
 736 E10009, doi:10.1029/2010JE003640.
- 737 Ulrich, M., Hauber, E., Herzsuh, U., Härtel, S., Schirrmeister, L., 2011. Polygon pattern
 738 geomorphology on Svalbard (Norway) and western Utopia Planitia (Mars) using high-
 739 resolution stereo remote-sensing data. *Geomorphology* 134, 3-4, 197-216, doi.org/10.
 740 1016/j.geomorph.2011.07.002.
- 741 Wan Bun Tseung, J.M., Soare, R.J., 2006. Thermokarst and related landforms in western
 742 Utopia Planitia, Mars. Implications for near-surface excess ice. 37th Lunar &
 743 Planetary Science Conference, 1414,
- 744 Wilson, L., Head, J.W., 2007. Explosive volcanic eruptions on Mars: Tephra and accretionary
 745 lapilli formation, dispersal and recognition in the geologic record. *Journal of*
 746 *Volcanology and Geothermal Research* 163, 83-97.

747 **Figures**

748 **Fig. 1:** Context maps of our study site. (a) Mars Orbiter Camera, wide angle mosaic of
 749 Utopia Planitia (*UP*), box indicates our region of study shown in (c-d). (b) *OMEGA*
 750 mosaic 0.77-1.30 μm spectral slope map of *UP*. (c) Mosaic of *CTX* images showing
 751 the area of study, red box indicates location of *HiRISE* image shown in Figure 2a-c,
 752 yellow hourglass footprints show locations of *CRISM* images shown in Figure 3. (d)
 753 *CTX* map with *OMEGA* spectral-slope map overlain.

754 **Fig. 2:** Putative periglacial-landforms (*PPLs*) at the mid-latitudes of *UP* and a thermokarst
 755 lake-alas complex on Earth. (a) *CTX* image overview of the periglacially-modified
 756 terrain (we suggest) in *UP*; the image shows the spatial relationship between light-
 757 toned (*LT*) and dark-toned (*DT*) terrain and materials. *CTX* image

758 P22_009467_2225_XN_42N273W (credit: NASA/JPL/MSSS). (b) Detail of the *PPLs*
 759 in *HiRISE* image with central colour-strip, showing the qualitative colour difference
 760 between the light-toned and dark-toned terrains. Terraces in the walls of the
 761 depressions are also visible (*tr*), as well as polygon margin and junction-pits (*p*).
 762 *HiRISE* image ESP_026385_2225; 42.305⁰ N, 86.49⁰ E (credit: NASA/JPL/UofA).
 763 (c) Close-up of a scalloped depression, with polygon-margin pits (*p*) and terraces (*tr*).
 764 *HiRISE* image ESP_026385_2225 (credit: NASA/JPL/UofA). (d) Oblique aerial-
 765 image of thermokarst lake and marginal small-sized polygons, some of whose troughs
 766 are filled with water (Tuktoyaktuk Coastlands, northern Canada). The thermokarst
 767 lake in the background is ~100m across. Image credit: R.J. Soare.

768 **Fig. 3:** *CRISM* observations in SW Utopia (a-c) *CRISM* footprints over *CTX* images showing
 769 scalloped depressions in *CRISM* image FRT0000A116 (credit: JHU/APL) (a), crater
 770 wall with exposed subsurface units in FRT00009A8B (b), and the bright toned mantle
 771 to the south in FRT000098DF (c). Numbered subpanels show surface texture and
 772 albedo in sampling areas for *CRISM* spectra, at locations indicated in A-C, from
 773 *HiRISE* images PSP_009467_2225 (42.223⁰ N, 86.321⁰ E), PSP_006606_2240
 774 (43.816⁰ E, 89.514⁰ E), and PSP_006962_2215 (41.322⁰ N, 90.095⁰ E, respectively
 775 (credit: NASA/JPL/UofA). (d-f) *CRISM* spectra from locations shown in (a-c),
 776 respectively, corresponding to the numbered locations.

777 **Fig. 4:** Laboratory spectra of Hawaiian basaltic glasses, Mauna Kea. All spectra have been
 778 scaled to one at their maximum value and are stacked for clarity. Points indicate
 779 spectra, lines are smoothed spectra. All spectra are sourced from the Planetary Data
 780 System unless otherwise noted. Data are not available for some spectra beyond 2.1
 781 μm . (a) Unaltered ash, showing both the spectrum of the bulk ash and size fractions
 782 (HWMK513). (b) Altered ash and glass. Top spectrum shows glass sand altered in the

783 laboratory (Horgan et al., 2013); next two spectra are naturally altered glassy cooling
 784 rinds (Minitti et al., 2007); bottom three spectra are naturally altered ashes
 785 (HWMK024, HWMK001, WP006). (c) Altered ash, showing the bulk spectrum
 786 compared to various size fractions (HWMK012). Larger-sized fractions resemble
 787 leached glass, consistent with laboratory leached glass sand (Horgan *et al.*, 2013), the
 788 smallest size fractions resemble palagonite (Singer, 1982), and intermediate size
 789 fractions are consistent with a combination of these two end members.

790 **Fig 5:** Examples from HiRISE red-channel images of possible layering in the walls of
 791 scalloped depressions, which also show polygonal terrain incised into the upper dark
 792 unit and drifts of dark sediments. (a) ESP_019950_2250 (44.719⁰ N, 88.500⁰ E) (b)
 793 ESP_025831_2260 (45.831⁰ N, 90.503⁰ E) (c) ESP_026385_2225 (42.305⁰ N,
 794 86.149⁰ E) (d) ESP_036499_2240 (43.795⁰ N, 83.367⁰ E) (credit: NASA/JPL/UofA).

795 **Fig. 6:** A photograph taken from the southern slopes of Tolbachik (photo grid ref: 55.792⁰ N,
 796 160.317⁰ E) looking SE. In the foreground, below the dotted line, the frame shows
 797 dark-toned volcanic sediments resulting from an eruption in 1975-76. Thermal-
 798 contraction cracks and the polygonised-terrain comprised of them are visible to the
 799 left and centre of the frame (insets a and b). Ice wedges, not directly visible in this
 800 frame, feed into melt-related groundwater drainage-channels (i); the latter drain
 801 towards the camera and then to the south, into the right of the frame. The volcanic
 802 cone in the background (ii) is the volcano 'Udina' (2920m/asl). Posky Tolbachik lies
 803 out of the frame to the left. Insets (a) and (b) have been colour-enhanced to bring out
 804 the polygonised-terrain. Image credit: Colin Souness.

805 **Fig. 7:** Schematic diagramme of possible ice-enrichment and the formation of excess ice in
 806 the dark-toned terrain observed by us at the mid-latitudes of *UP*. (a) Dark-toned,
 807 relatively fine-grained and frost-susceptible volcanic sediments are emplaced,

808 blanketing the landscape in *UP*. (b) These sediments are superposed by
809 atmospherically precipitated snow and/or ice, either under enhanced obliquity-
810 conditions or under climate-excursions caused by the volcanic perturbations. (c) The
811 surface ice/snow is redistributed to depth by thaw, meltwater percolation, freezing and
812 the formation of ice-rich structures in the sediment column. Stages (a-c) or (b-c) can
813 be repeated as often as climatic/volcanic conditions allow. (d) Once emplaced, the
814 near-surface ice-rich sediments are subjected episodically to thermal-contraction
815 cracking and localised thermal-destabilisation, forming the triumvirate of *PPLs*
816 discussed earlier.

Highlights

Suites of putative periglacial landforms (*PPLs*) occur in mid Utopia Planitia

On Earth, similar assemblages form in ice-enriched permafrost by freeze-thaw cycling

OMEGA/CRISM data show that the *PPLs* occur in frost-susceptible volcanic terrain

Similar terrain in Kamchatka frames this data in a 3-stage ice-enrichment hypothesis

Figure

[Click here to download high resolution image](#)

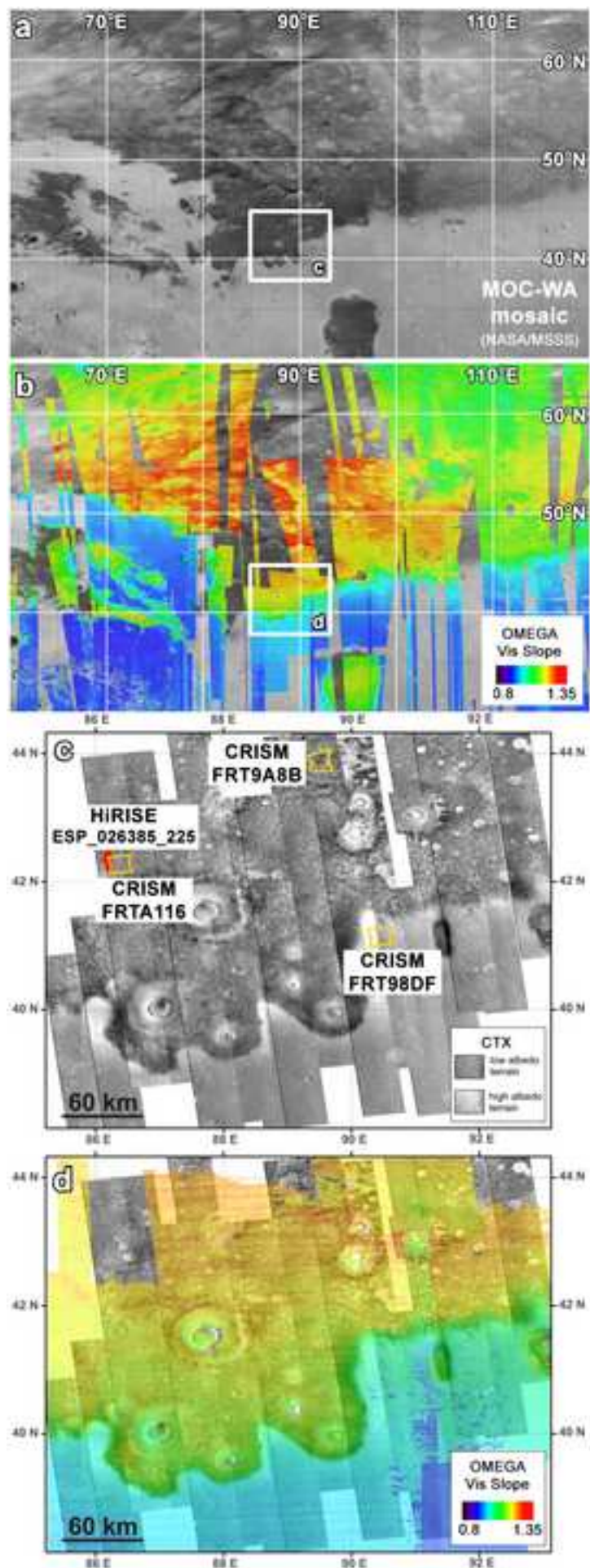
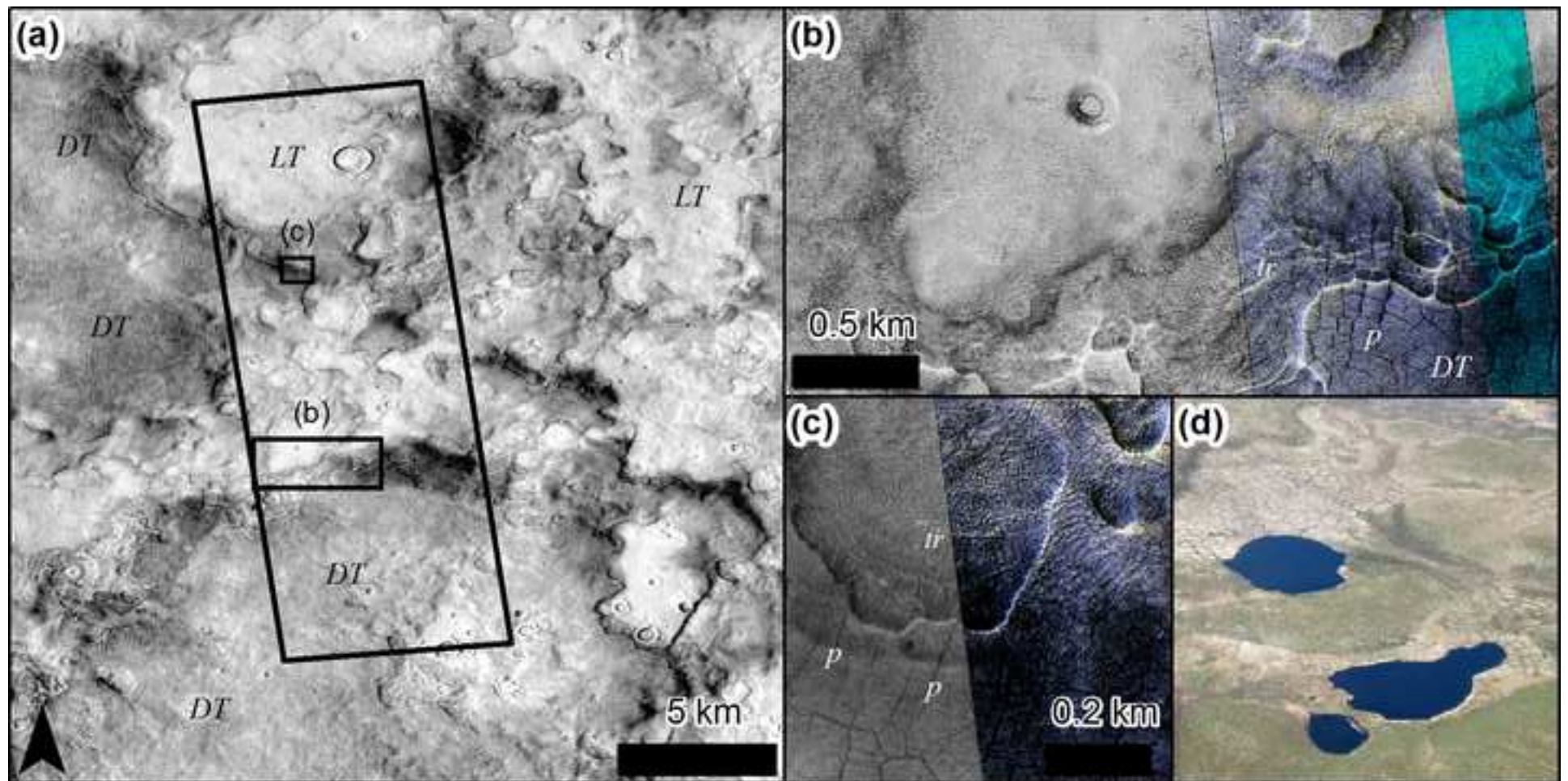
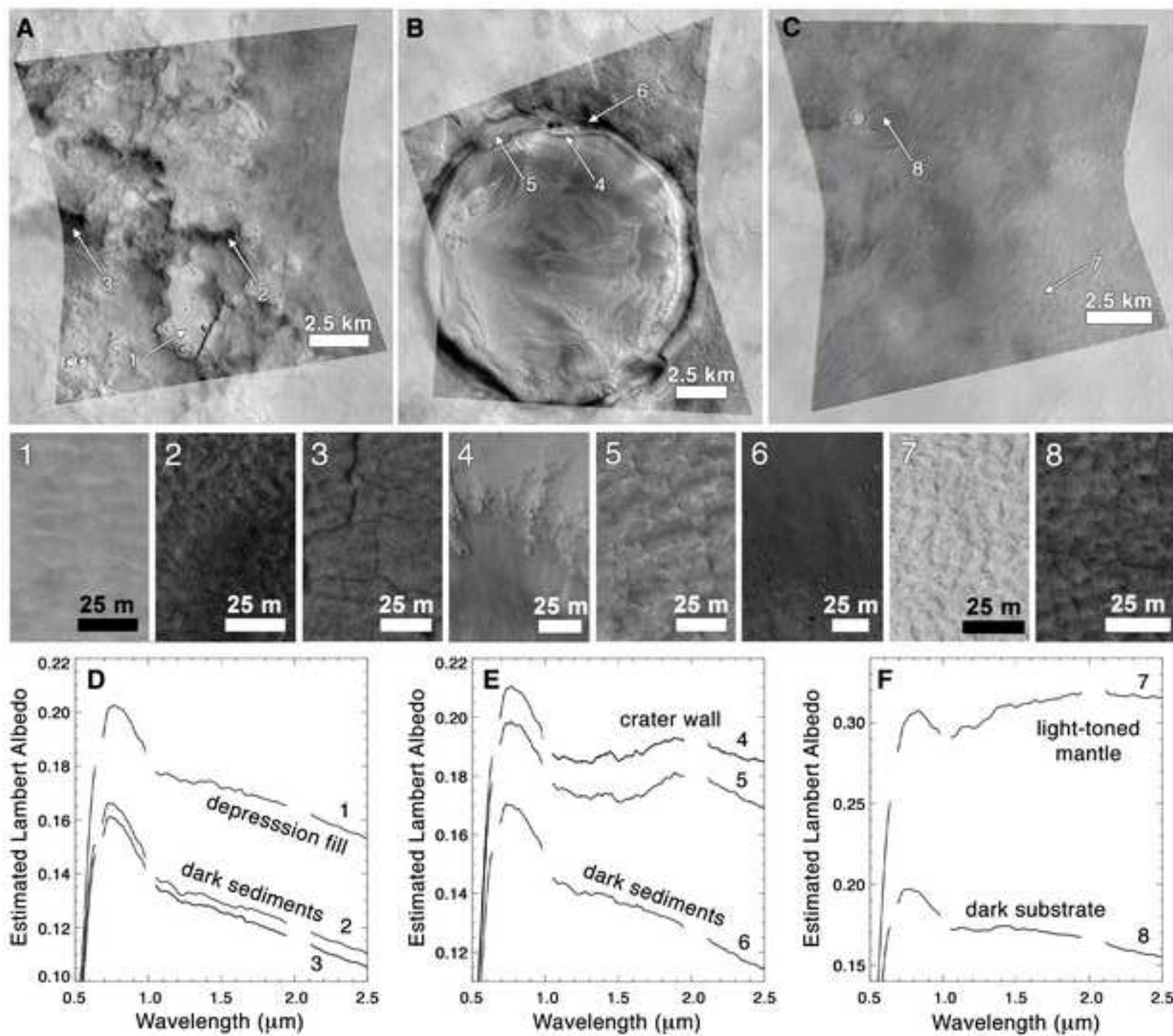


Figure
[Click here to download high resolution image](#)



Figure

[Click here to download high resolution image](#)



Figure

[Click here to download high resolution image](#)

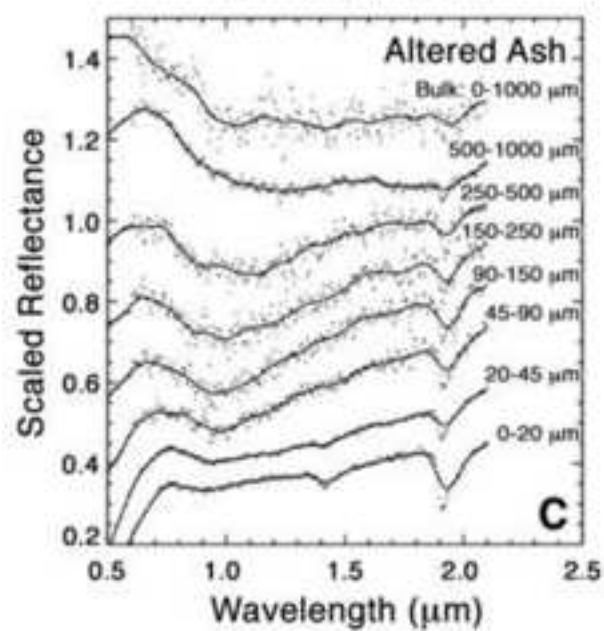
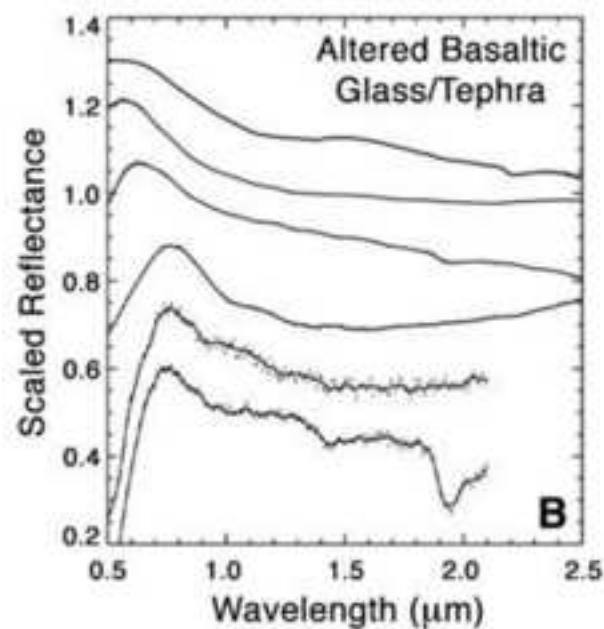
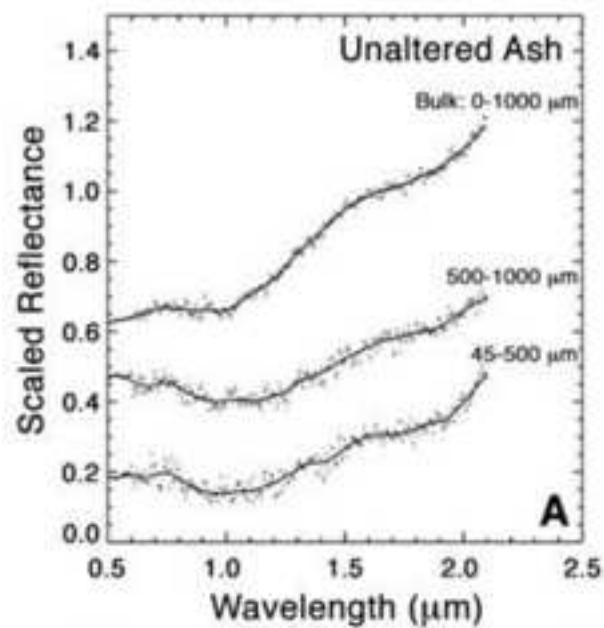
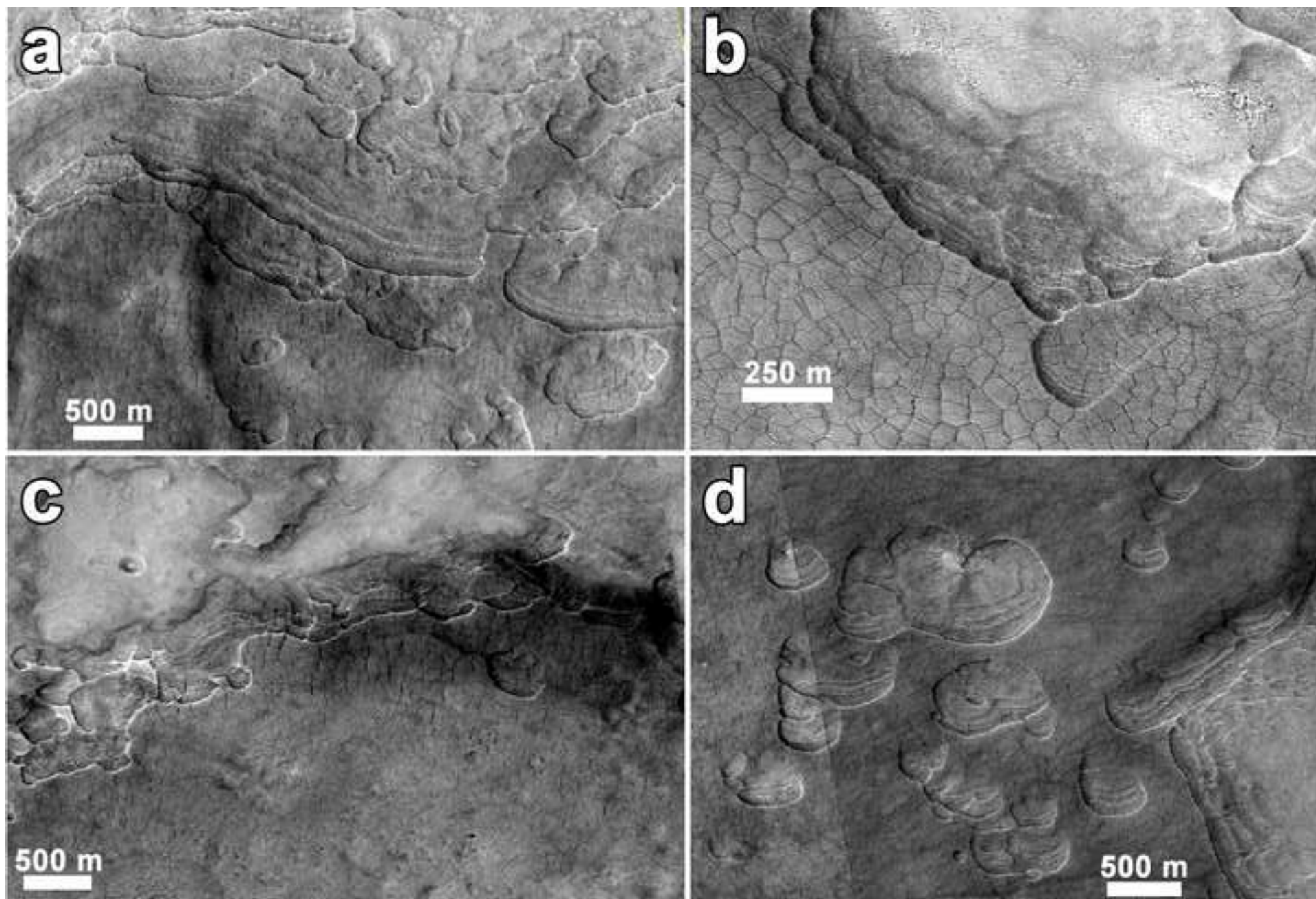
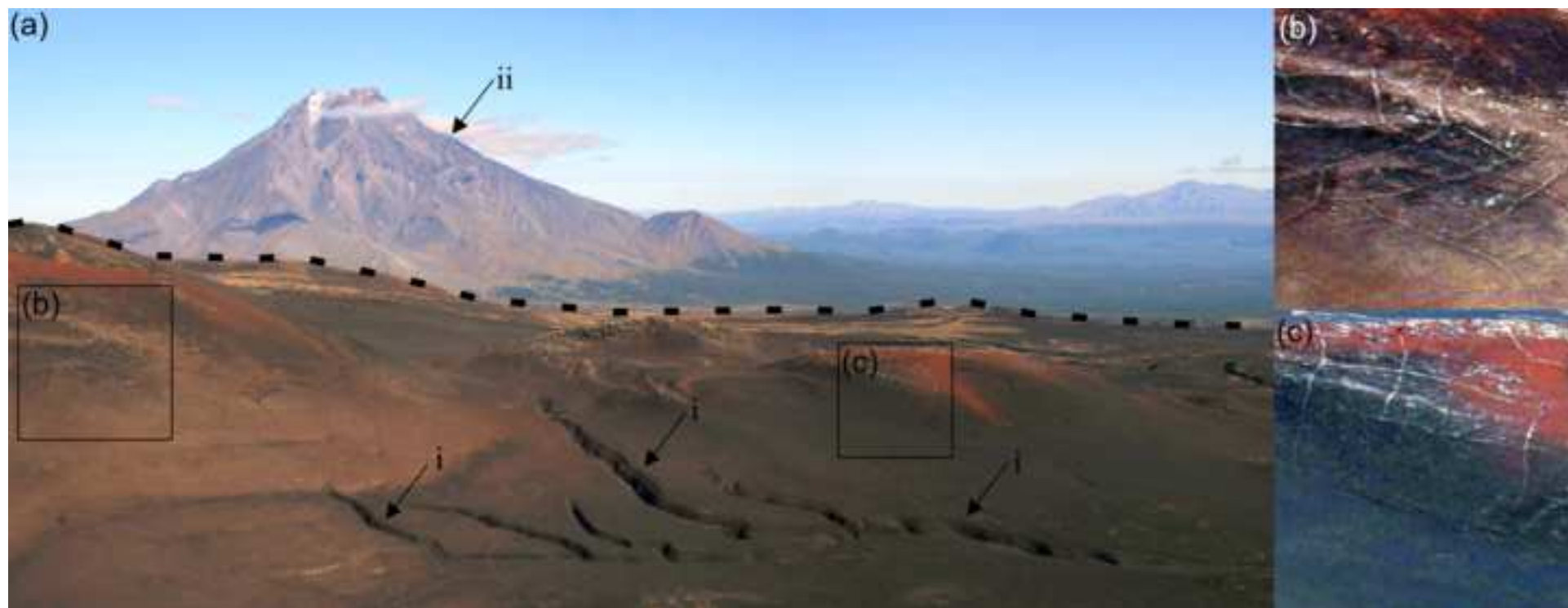


Figure
[Click here to download high resolution image](#)



Figure

[Click here to download high resolution image](#)



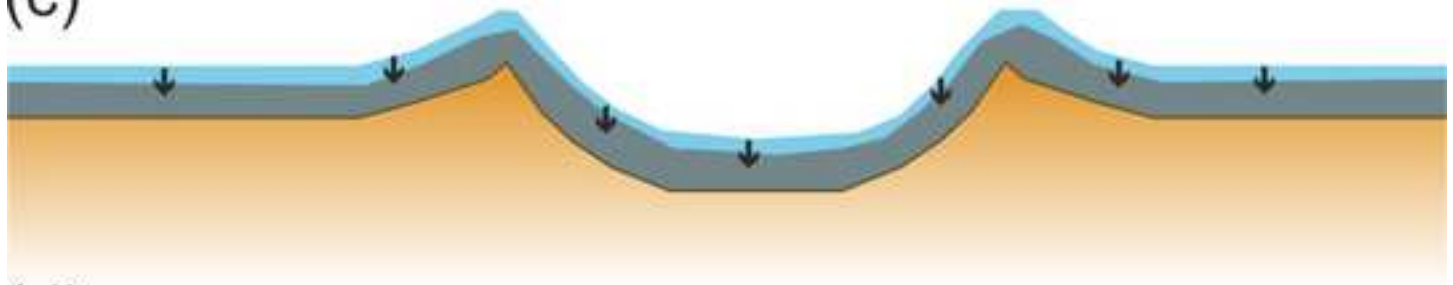
(a)



(b)



(c)



(d)

